TECHNISCHE MECHANIK
an open access journal

journal homepage: www.ovgu.de/techmech

Tech. Mech., Vol. 45, Is. 1, (2025), 46–62

Received: 08.11.2024
Accepted: 01.07.2025
Available online: 08.07.2025

Influence of Magnetic Field Dependent Viscosity on Thermal Instability in a Ferrofluid Layer Saturating a Porous Medium with Permeable Boundaries

Abhishek Thakur, Pankaj Kumar, Awneesh Kumar and Mandeep Kaur

Central University of Himachal Pradesh, Shahpur, Himachal Pradesh, 176206, India

Abstract: In this study, we explore the stability of a ferrofluid layer saturating a densely packed porous medium, situated between two horizontal permeable boundaries, influenced by magnetic-field-dependent (MFD) viscosity and a vertically oriented magnetic field. The analysis is carried out using linear stability theory and the normal mode method to derive the eigenvalue problem. A single-term Galerkin method is adopted for solving the eigenvalue problem, facilitating the calculation of critical wave number and critical magnetic Rayleigh number and for distinct boundary combinations. The principle of exchange of stabilities is upheld, indicating that convection begins solely via the stationary mode. Through numerical calculations and graphical representations, the study evaluates the impact of various important factors, such as the MFD viscosity parameter, medium permeability, permeable boundary parameters, and magnetic parameters M_1 and M_3, on the initiation of stationary convection. The findings reveal that the viscosity stabilizes the system across all boundary combinations, while medium permeability destabilizes it. Furthermore, the transition in the nature of permeable boundaries from rigid to free results in an increase in the magnetic Rayleigh number, indicating that convection occurs later in the former case, which corresponds to greater stability in the system. These results are essential for advancing various industrial, engineering and environmental applications involving convection in ferrofluids.

Keywords: Convection, permeable boundaries, Galerkin method, MFD viscosity, porous medium

1 Introduction

Ferrofluids are colloidal suspensions of magnetically responsive nanoparticles, such as cobalt ferrite or iron oxide dispersed in carrier fluids like hydrocarbon-based solvents or water. Ferrofluid was invented by NASA's scientist Steve Papell in 1963 to create rocket fuel. These fluids have diversified into engineering, medicine, and electronics. They feature solid magnetic particles (3-15 nm) individually coated with dispersants, ensuring stable suspension in liquid mediums. Due to Brownian motion, these particles remain uniformly distributed and do not settle under normal conditions, ensuring stability of flow. Their presence modifies the viscosity and thermal conductivity of the base fluid, thereby influencing heat transfer, flow resistance, and magneto-convective behavior. Noteworthy for their magnetization saturation, high susceptibility, and superparamagnetism, ferrofluids find extensive use in magnetic sealing, damping, drug delivery, loudspeakers, and electronics cooling. They also serve in diverse fields like MRI, shock absorption, soft robotics, microfluidics, avionics, and actuators. Evolving applications in damping technologies, influenced by magnetic field strength and shear viscosity changes, promise future advancements (Rosensweig (1997); Odenbach and Thurm (2002)).

In recent decades, extensive scientific studies have been undertaken to explore the process of convection in these fluids passing through porous media under different effects and configurations (Nield and Bejan (2006); Sharma et al. (2009); Nanjundappa et al. (2014); Keene and Goldstein (2015)). The magnetic attributes of the ferrofluid, the structural characteristics of the porous material, and external influences such as gravity and magnetic fields all play a crucial role in shaping the flow patterns and heat transfer features. he study of convective instability in ferrofluids subjected to bottom heating and an upward-directed magnetic field was pioneered by Finlayson (1970), who incorporated the role of gravity and evaluated both free and rigid boundary conditions, deriving exact as well as approximate results. Building on this, Lalas and Carmi (1971) analyzed the stability behavior of a Boussinesq-type magnetic fluid by accounting for thermal gradients, magnetic influence, and gravitational effects. Later, Shliomis (1974) explored ferroconvection instability under the influence of a magnetic field, particularly for systems with free boundaries. In a related experimental framework, Schwab et al. (1983) investigated the onset of instability in a magnetic fluid layer within the classical Bénard setup, where a vertical magnetic field was applied. Their approach involved measuring the effective thermal conductivity to estimate the threshold temperature difference. Stiles and Kagan (1990) investigated the thermoconvective instability in a horizontal ferrofluid layer subjected to a strong vertical magnetic field, highlighting discrepancies between experimental results and theoretical predictions based on Finlayson's model. Later, Venkatasubramanian and Kaloni (1994) explored the effect of rotation on the thermoconvective instability of a horizontal ferrofluid layer and found that rotation stabilizes the system, though at a slower rate compared to ordinary viscous fluids, with the extent of stabilization depending significantly on the type of boundary conditions. Numerous studies, both experimental and theoretical, have been conducted in the literature to investigate the thermal convection in ferrofluids (Mahajan and Arora (2013); Selimefendigil and Öztop (2015); Kpossa and Monwanou (2022); Ram et al. (2022)). Recent advancements in magnetohydrodynamics (MHD) flow analysis

* E-mail address: pankajthakur28.85@hpcu.ac.in doi: 10.24352/UB.OVGU-2025-040

have increasingly focused on more realistic and application-driven scenarios, such as non-uniform geometries, variable fluid properties, and advanced modeling approaches. Analytical solutions have been developed by Ellahi (2013) to examine the impact of temperature-dependent viscosity on non-Newtonian nanofluid flow in pipes under magnetic fields, reinforcing the importance of variable fluid properties in thermal engineering. The influence of quadratic thermal radiation on nanofluid flow over a stretching sheet with variable thickness has been explored by Nihaal et al. (2025) using the Xue and Yamado-Ota thermophysical model, offering improved accuracy in thermal analysis. Similarly, the role of the Richardson number in inclined MHD mixed convection has provided deeper insights into combined heat and mass transfer behavior Mahabaleshwar et al. (2024). Studies on couple stress nanofluid flow over porous stretching and shrinking surfaces have contributed to a better understanding of microscale effects in heat transfer Vishalakshi et al. (2024). Furthermore, the integration of machine learning and artificial intelligence with MHD flow models, such as in the analysis of Jeffrey nanofluids over exponentially stretching sheets, highlights the growing use of data-driven methods in fluid mechanics Zeeshan et al. (2024). For further insights into such developments, one may refer to the contributions made by numerous researchers across the field (Sachhin et al. (2023); Vishalakshi et al. (2023); Mahabaleshwar et al. (2022)).

The thermal convection behavior in ferromagnetic fluids is heavily shaped by their intrinsic physical properties. Notably, parameters such as viscosity and its dependence on temperature play a central role, as they are influenced by both magnetic and hydrodynamic interactions. In the context of stress-free boundary conditions, Mahajan and Sharma (2014) conducted a nonlinear stability analysis considering magnetic-field-dependent (MFD) viscosity effects in ferrofluids. Further developments in this area include the work of Sheikholeslami et al. (2016), who investigated the influence of variable MFD viscosity on natural convection within nanofluids. In another contribution, Prakash et al. (2018a) focused on the role of MFD viscosity in modulating thermal convection within a magnetized fluid layer subjected to an upward magnetic field. More recently, Molana et al. (2020) examined a novel enclosure geometry filled with Fe_3O_4-water nanofluids, assessing convection under a constant, inclined magnetic field. Additionally, Shree et al. (2022) studied buoyancy-induced convection phenomena in a porous medium saturated with ferrofluid, incorporating both MFD viscosity and the Maxwell–Cattaneo thermal flux model. The study of fluids in magnetohydrodynamics is now being extended to explore complex behaviors with different effects along with advanced modeling approaches. Kumari et al. (2024) studied the combined effect of temperature gradient and electric field on a horizontal viscoelastic fluid layer with an internal heat source or sink. To better understand how viscosity interacts with other important factors in the study of ferroconvection, one can look into the work done by several researchers in this area (Ram et al. (2010); Zeidan et al. (2014); Izadi et al. (2020); Ram et al. (2021); Kumar et al. (2024a)).

In addition to the inherent properties of ferrofluids, the nature of boundary surfaces, particularly their permeability, plays a vital role in governing convection, as it allows for the exchange of both mass and heat across the boundaries. Over recent decades, increasing emphasis has been placed on both theoretical and applied research concerning fluid flow, heat, and mass transport within porous media due to its wide-ranging engineering applications. Vafai (1984) explored how inertial effects and porosity influence convective behavior within porous structures. In a notable study, Siddheshwar (1995) analyzed thermal magnetic convection in an infinitely extended ferrofluid layer with magnetically permeable boundaries, specifically under the condition where the permeabilities of both surfaces were equal. The existence of hydrodynamic instability in a bottom-heavy configuration with porous boundaries was later confirmed by Gupta and Shandil (2011). Furthermore, Vafai (2015) highlighted that the diverse nature of porous materials significantly affects flow behavior and transport phenomena. More recently, Surya and Gupta (2022) examined how variations in gravitational acceleration influence the onset of thermal instability in conventional fluid layers bounded by permeable surfaces. Within the same boundaries, Kumar et al. (2024b, 2025) investigated the onset of thermal convection in ferromagnetic fluid layers. The first study focused on a dusty fluid influenced by temperature-dependent viscosity, while the second examined the impact of MFD viscosity in a sparsely dispersed porous medium.

Despite the growing literature on ferroconvection, recent contributions have addressed many aspects individually, but a comprehensive study that incorporates MFD viscosity, magnetization within permeable boundary configurations in a porous medium remains absent. The present study aims to bridge this gap by considering the combined effect of these significant parameters and realistic permeable boundary surfaces on the instability behavior of ferrofluids in porous domains. These factors lead to interdependent relationships between magnetic effects, viscosity variations, and boundary conditions, making analytical treatment both challenging and meaningful. To tackle this, a single-term Galerkin method is employed to solve the resulting eigenvalue problem under permeable boundary conditions. The analysis offers a detailed exploration of how MFD viscosity, medium permeability, and magnetic parameters govern the stability characteristics of the system, with results presented through systematic graphical interpretation.

2 Mathematical Description of the Problem

Consider an infinitely extended horizontal layer of Boussinesq magnetic fluid confined statically between permeable boundaries at a finite vertical distance d apart, and experiencing heating from the lower boundary. The magnetic fluid layer is electrically non-conducting and incompressible, and its viscosity is taken as $\mu = \mu_1 \left(1 + \vec{\delta} \cdot \vec{B}\right)$ (Prakash et al. (2018b)), where μ and μ_1 are the respective viscosities of the ferrofluid in the presence and absence of a magnetic field. The variable δ represents the MFD viscosity parameter. Throughout the analysis, we will refer to δ as the viscosity parameter. Here, δ is isotropic and has the same value as $\delta_1 = \delta_2 = \delta_3 = \delta$. A linear variation of magnetoviscosity has been employed as an initial estimate for small field variations. A uniform temperature gradient β is sustained across the fluid layer, with the upper and lower permeable boundaries held at temperatures T_1 $(T_1 < T_0)$ and T_0, respectively. The system is influenced by gravitational acceleration represented as $\vec{g} = (0, 0, -g)$, while a uniform magnetic field $\vec{H}$ is applied in the upward vertical direction (see Fig. 1).

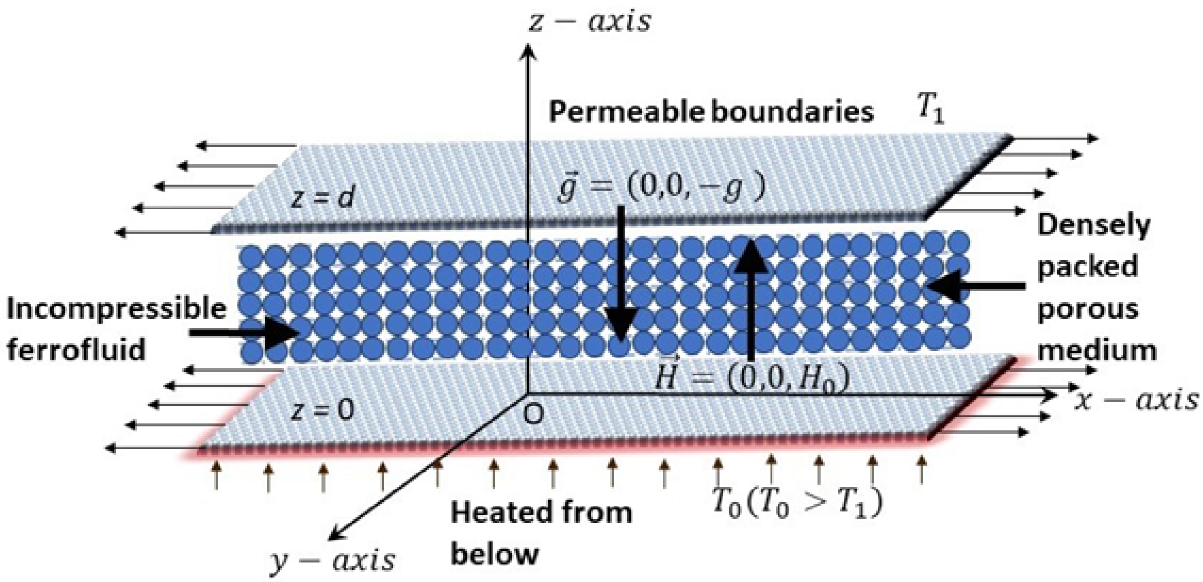

Fig. 1: Geometrical set up of the physical configuration.

The mathematical model describing the present physical system is governed by the following set of equations, as formulated in earlier works (Finlayson (1970); Prakash et al. (2018a)):
The continuity equation is expressed as

$$\nabla \cdot \vec{q} = 0. \tag{1}$$

The equation of motion is given by

$$\frac{\rho_0}{\epsilon}\left(\frac{\partial}{\partial t} + \frac{1}{\epsilon}(\vec{q}.\nabla)\right)\vec{q} = \rho\vec{g} - \nabla p + \nabla \cdot \left(\vec{H}\,\vec{B}\right) + \frac{\mu}{k_0}\vec{q}. \tag{2}$$

The temperature equation is

$$\epsilon\left[\rho_0 C_{H,V} - \mu_0 \vec{H} \cdot \left(\frac{\partial \vec{M}}{\partial T}\right)_{H,V}\right]\frac{dT}{dt} + (1-\epsilon)\,\rho_s C_s \frac{dT}{dt} + T\mu_0\left(\frac{\partial \vec{M}}{\partial T}\right)_{H,V} \cdot \frac{d\vec{H}}{dT} = \kappa\nabla^2 T + \Phi, \tag{3}$$

where $\vec{q} = u\hat{i} + v\hat{j} + w\hat{k}$ is velocity of ferrofluid, $\rho = \rho_0\,(1 + \alpha\,(T_0 - T))$ is density of the ferrofluid, ρ_0 is density at temperature T_0, α is volume expansion coefficient, ϵ is medium porosity, μ_0 is magnetic permeability, k_0 is medium permeability, $\vec{H}$ represents magnetic field, p is pressure, μ denotes variable viscosity, $C_{H,V}$ represents heat capacity with both magnetic field and volume held constant, $\vec{M}$ is magnetization, T is temperature, Φ refers to viscous dissipation that involves second-order velocity terms, and κ is thermal conductivity.
In case of a non-conducting fluid and in the absence of displacement current, the Maxwell's equations are

$$\nabla \times \vec{H} = 0 \tag{4}$$

and

$$\nabla \cdot \vec{B} = 0, \tag{5}$$

where $\vec{B}$ is given by

$$\vec{B} = \mu_0\left(\vec{H} + \vec{M}\right). \tag{6}$$

Considering the parallel orientation of magnetization and the magnetic field, as well as dependence of magnetization on magnetic field intensity and temperature, the magnetization can be expressed as (Finlayson (1970))

$$\vec{M} = M\left(\frac{\vec{H}}{H}\right)(H, T). \tag{7}$$

The equation describing the linearized magnetic state is given as follows

$$M = M_0 + K_2\,(T_0 - T) - \chi\,(H_0 - H), \tag{8}$$

where M_0 represents the magnetization at a specific magnetic field strength H_0 and temperature T_0. The pyromagnetic coefficient, denoted as K_2, is defined as $K_2 = -\left(\frac{\partial \vec{M}}{\partial T}\right) T_0, H_0$, while $\chi = \left(\frac{\partial \vec{M}}{\partial \vec{H}}\right) T_0, H_0$ quantifies the material's magnetization response to an external magnetic field.
The analysis is influenced only by the spatially varying components of M_0 and H_0, making the orientation of the external magnetic field insignificant, and convection remains unchanged regardless of whether the magnetic field aligns with or opposes the gravitational force (Finlayson (1970)).
In a quiescent state, the solutions are presented as follows

$$\begin{aligned}&\vec{q} = \vec{q}_b = 0, \quad T = T_b(z) = -z\beta + T_0, \quad \rho = \rho_b(z), \quad \beta = \frac{T_0 - T_1}{d}, \quad p = p_b(z)\\ &\vec{M}_b = \left(M_0 + \frac{K_2\beta z}{\chi + 1}\right)\hat{k}, \quad \vec{H}_b = \left(H_0 - \frac{K_2\beta z}{\chi + 1}\right)\hat{k}, \quad M_0 + H_0 = H_0^{ext},\end{aligned} \tag{9}$$

where $\hat{k}$ represents the unit vector that points along the $z-$axis.

Following Finlayson (1970), we proceed to assess the stability of the quiescent stage by setting the perturbations described below

$$\begin{aligned}&\rho = \rho_b(z) + \rho', \quad p = p_b(z) + p', \quad \vec{q} = \vec{q'} = u'\hat{i} + v'\hat{j} + w'\hat{k}, \quad T = T_b(z) + \theta',\\ &\vec{M} = \vec{M}_b(z) + \vec{M}', \quad \vec{H} = \vec{H}_b(z) + \vec{H}',\end{aligned} \tag{10}$$

where ρ', p', $\vec{q'} = u'\hat{i} + v'\hat{j} + w'\hat{k}$, θ', $\vec{M}'$ and $\vec{H}'$ are small perturbations in density, pressure, velocity, temperature, magnetization, and magnetic field respectively.
By plugging Eq. (10) into Eqs. (1) -(8) along with the utilization of basic state solutions provided by Eq. (9), we obtain

$$\frac{\partial u'}{\partial x} + \frac{\partial v'}{\partial y} + \frac{\partial w'}{\partial z} = 0, \tag{11}$$

$$\frac{\rho_0}{\epsilon}\frac{\partial u'}{\partial t} = -\frac{\partial p'}{\partial x} + \mu_0(M_0 + H_0)\frac{\partial H_1'}{\partial z} - \frac{\mu_1\left[1 + \delta\mu_0(M_0 + H_0)\right]}{k_0}u' \tag{12}$$

$$\frac{\rho_0}{\epsilon}\frac{\partial v'}{\partial t} = -\frac{\partial p'}{\partial y} + \mu_0(M_0 + H_0)\frac{\partial H_2'}{\partial z} - \frac{\mu_1\left[1 + \delta\mu_0(M_0 + H_0)\right]}{k_0}v' \tag{13}$$

$$\begin{aligned}\frac{\rho_0}{\epsilon}\frac{\partial w'}{\partial t} = &- \frac{\partial p'}{\partial z} + \mu_0(M_0 + H_0)\frac{\partial H_3'}{\partial z} + \rho_0\alpha\theta' g - \mu_0 K_2\beta H_3' - \frac{\mu_1}{k_0}w'\\ &+ \frac{\mu_0 K_2^2\beta\theta'}{\chi + 1} - \frac{\mu_1}{k_0}\delta\mu_0(M_0 + H_0)w',\end{aligned} \tag{14}$$

$$\rho C_1\frac{\partial \theta'}{\partial t} = \kappa\nabla^2\theta' + \mu_0 T_0 K_2\frac{\partial}{\partial t}\left(\frac{\partial \phi'}{\partial z}\right) + \left(\rho C_2\beta - \frac{\mu_0 T_0 K_2^2\beta}{\chi + 1}\right)w', \tag{15}$$

where $\rho C_1 = \epsilon\rho_0 C_{H,V} + \epsilon\mu_0 H_0 K_2 + (1 - \epsilon)\rho_s C_s$
and $\rho C_2 = \epsilon\rho_0 C_{H,V} + \epsilon\mu_0 H_0 K_2$
Now,

$$\frac{\partial}{\partial x}\left(M_1' + H_1'\right) + \frac{\partial}{\partial y}\left(M_2' + H_2'\right) + \frac{\partial}{\partial z}\left(M_3' + H_3'\right) = 0, \tag{16}$$

and

$$\vec{H}' = \nabla\phi', \tag{17}$$

where ϕ' represents the magnetic potential in perturbed state.

$$M_3' + H_3' = H_3'(\chi + 1) - K_2\theta', \tag{18}$$

$$M_i' + H_i' = \left(\frac{M_0}{H_0} + 1\right)H_i', (\text{where} \quad i = 1, 2), \tag{19}$$

where it is supposed that $\beta K_2 d \ll H_0 (\chi + 1)$.
By making use of Eq.(11) to eliminate u', $v\prime$, and $p\prime$ from Eqs.(12)–(14), the resulting expression is obtained as follows:

$$\frac{\rho_0}{\epsilon}\left(\frac{\partial}{\partial t}\nabla^2 w'\right) = \rho_0 \alpha g \nabla_1^2 \theta' - \mu_0 K_2 \beta \frac{\partial}{\partial z}\left(\nabla_1^2 \phi'\right) - \frac{\mu_1\left[1 + \delta\mu_0 \left(M_0 + H_0\right)\right]}{k_0}\frac{\partial^2 w'}{\partial z^2} + \frac{\mu_0 K_2^2 \beta \nabla_1^2 \theta'}{\chi + 1} - \frac{\eta_1}{k_0}\nabla_1^2 w' + \frac{\mu_1}{k_0}\delta\mu_0 \left(M_0 + H_0\right)\nabla_1^2 \left(w'\right). \tag{20}$$

Eqs. (16)–(19) are combined to yield the following result

$$(\chi + 1)\frac{\partial^2 \phi'}{\partial z^2} + \left(\frac{M_0}{H_0} + 1\right)\nabla_1^2 \phi' - K_2 \frac{\partial \theta'}{\partial z} = 0. \tag{21}$$

By applying normal mode analysis, the perturbed variables are expressed as

$$\left(w', \theta', \theta'\right)(x, y, z, t) = \left(w''(z), \theta''(z), \phi''(z)\right) e^{i\left(x k_x + y k_y\right) + nt}, \tag{22}$$

where $k = \sqrt{(k_x)^2 + (k_y)^2}$ is the wave number of the disturbance and n is constant which can be complex (Chandrasekhar (2013)).

The system of equations (22) is substituted into Eqs. (16), (20), and (21), followed by the non-dimensionalization of the variables through an appropriate scaling procedure, as outlined by Prakash et al. (2018a).

$$w^* = \frac{d}{\nu}w'', \quad z^* = \frac{z}{d}, \quad a = kd, \quad D' = Dd, \quad \nu = \frac{\mu_1}{\rho_0}, \quad k_0^* = \frac{k_0}{d^2}, \quad \theta^* = \frac{a R^{1/2} \kappa}{\beta \nu d \rho C_2}\theta'',$$
$$\phi^* = \frac{(\chi + 1)\kappa a R^{1/2}}{\rho C_2 \beta \nu d^2 K_2}\phi'', \quad \omega = \frac{n d^2}{\nu}, \quad P_r = \frac{\nu \rho C_1}{\kappa}, \quad P_r{}' = \frac{\nu \rho C_2}{\kappa}, \quad R = \frac{\rho C g \alpha \beta d^4}{\nu \kappa},$$
$$\delta^* = \mu_0 \delta H_0 (\chi + 1), \quad M_1 = \frac{\mu_0 K_2^2 \beta}{(\chi + 1)\alpha \rho_0 g}, \quad M_2 = \frac{\mu_0 K_2^2 T_0}{(\chi + 1)\rho C}, \quad M_3 = \frac{1 + \frac{M_0}{H_0}}{(\chi + 1)}. \tag{23}$$

Hence, for the sake of simplicity, the asterisks denoting non-dimensional variables are omitted in the subsequent expressions

$$\left(\frac{\omega}{\epsilon} + \frac{\delta M_3 + 1}{k_0}\right)\left(D^2 - a^2\right) w = a\sqrt{R}\left(D\phi M_1 - (M_1 + 1)\theta\right), \tag{24}$$

$$D^2\theta - \left(P_r \omega + a^2\right)\theta + P_r{}' M_2 \omega D\phi = (M_2 - 1)\sqrt{R} a w, \tag{25}$$

$$\left(D^2 - a^2 M_3\right)\phi - D\theta = 0. \tag{26}$$

In this analysis, the spatial variable z is considered real and confined to the domain $[0, 1]$. The symbol a denotes the wave number, while D indicates differentiation with respect to z. The dimensionless numbers P_r and R, both strictly positive, represent the Prandtl and Rayleigh numbers, respectively. Magnetic influences are incorporated through the parameters M_1 and M_2, which capture the relative contribution of magnetically induced thermal flux to the overall magnetic flux. The parameter M_3, also positive, accounts for the nonlinear characteristics of magnetization. Furthermore, the growth rate ω is treated as a complex quantity, expressed as $\omega = \omega_r + i\omega_i$, where ω_r and ω_i are real-valued components corresponding to the real and imaginary parts. Also, $\theta = (\theta_r, \theta_i), w = (w_r, w_i)$ and $\phi = (\phi_r, \phi_i)$ are complex-valued functions dependent on variable z.
As the parameter M_2 is known to be exceedingly small (Finlayson (1970)), its influence is considered insignificant for the current study and thus omitted from the subsequent lateral analysis. Accordingly, Eq. (25) is modified and takes the following form:

$$D^2\theta - \left(P_r \omega + a^2\right)\theta = -\sqrt{R} a w. \tag{27}$$

The solutions of the perturbed system are further subject to boundary conditions specified at two distinct permeable interfaces: the lower boundary located at $z = 0$ and the upper boundary at $z = 1$. As both boundaries are assumed to be stationary, the following conditions hold:

$$\theta = 0 = w \quad \text{at} \quad z = 0,\ 1 \tag{28}$$

To characterize the permeability of the boundary surfaces in the present analysis, the following boundary conditions are employed, as originally proposed by Beavers and Joseph (1967)

$$D^2w - K_0 Dw = 0 \quad \text{at} \quad z = 0, \tag{29}$$

$$D^2w + K_1 Dw = 0 \quad \text{at} \quad z = 1. \tag{30}$$

The parameters $K_0 = \frac{\epsilon_0 d}{k_1}$ and $K_1 = \frac{\epsilon_1 d}{k_2}$ characterize the effective permeability at the lower and upper boundaries, respectively. Here, ϵ_0 and ϵ_1 are dimensionless coefficients that encapsulate the physical properties of the porous interface materials, while k_1 and k_2 are representative length scales associated with the boundary layer permeability.

In the limiting case where the magnetic susceptibility $\chi \to \infty$, corresponding to a highly magnetically responsive medium (Finlayson (1970)), the magnetic potential ϕ satisfies the following boundary conditions:

$$D\phi = 0 \quad \text{at} \quad z = 0,\ 1. \tag{31}$$

The system defined by Eqs. (24), (26), and (27), subject to the boundary constraints (28)–(31), constitutes a well-posed eigenvalue problem.

2.1 The Principle of Exchange of Stabilities (PES)

The PES is a foundational concept in linear stability theory, particularly relevant to the study of thermomagnetic convection. It posits that, at the threshold of instability, the transition from the base state to the convective state occurs without oscillations that is, through stationary (non-oscillatory) modes. This assumption simplifies the mathematical treatment of the problem.
To assess the validity of PES in the context of the present model, we utilize the classical approach introduced by Pellew and Southwell (1940), which remains one of the most widely accepted methods for verifying whether this principle holds. Their methodology provides a criterion for distinguishing between stationary and oscillatory modes at the onset of convection, thereby offering a means to evaluate the appropriateness of applying PES.

To proceed with this, Eq. (24) is multiplied by the complex conjugate of w, denoted by w^*, and the resulting expression is integrated over the domain $z \in [0, 1]$

$$\left[\frac{\omega}{\epsilon} + \frac{(\delta M_3 + 1)}{k_0}\right] \int_0^1 w^* \left(D^2 - a^2\right) w dz = a\sqrt{R}\left[M_1 \int_0^1 w^* D\phi dz - (M_1 + 1) \int_0^1 w^* \theta dz\right]. \tag{32}$$

By appropriately applying the boundary conditions given in Eqs. (28)–(31) and performing the necessary number of integrations on each term in Eq. (32), we arrive at the following simplified form

$$\begin{aligned} -\left[\frac{\omega}{\epsilon} + \frac{(\delta M_3 + 1)}{k_0}\right] \int_0^1 \left(a^2 |w|^2 + |Dw|^2\right) dz &= M_1 \int_0^1 \left(a^2 M_3 |D\phi|^2 + \left|D^2\phi\right|^2\right) dz \\ &+ M_1 \left(a^2 + P_r \omega^*\right) \int_0^1 \left(a^2 M_3 |\phi|^2 + |D\phi|^2\right) dz \\ &- (M_1 + 1) \int_0^1 \left(\left(a^2 + P_r \omega^*\right) |\theta|^2 + |D\theta|^2\right) dz. \end{aligned} \tag{33}$$

Substituting $\omega = \omega_r + i\omega_i$ and $\omega^* = \omega_r - i\omega_i$ in Eq. (33) and comparing the imaginary terms, we get

$$\omega_i \left[\int_0^1 \left(a^2 |w|^2 + |Dw|^2 + \epsilon (M_1 + 1) P_r |\theta|^2 - \epsilon M_1 P_r \left(a^2 M_3 |\phi|^2 + |D\phi|^2\right)\right) dz\right] = 0. \tag{34}$$

Multiplying Eq. (26) by ϕ^* and taking integration from $z = 0$ to $z = 1$, we get

$$\int_0^1 \phi^* \left(D^2 - a^2 M_3\right) \phi dz = \int_0^1 \phi^* D\theta dz \tag{35}$$

Further, Eq. (35) is simplified to

$$\begin{aligned} \int_0^1 \left(a^2 M_3 |\phi|^2 + |D\phi|^2\right) dz &= \int_0^1 \theta D\phi^* \, dz \\ &\leq \int_0^1 |D\phi|\, |\theta| \, dz \\ &\leq \left[\int_0^1 |D\phi|^2 \, dz\right]^{1/2} \left[\int_0^1 |\theta|^2 \, dz\right]^{1/2}. \end{aligned} \tag{36}$$

(using Schwarz's inequality)

It follows that

$$\int_0^1 |D\phi|^2 \, dz \leq \left[\int_0^1 |D\phi|^2 \, dz\right]^{1/2} \left[\int_0^1 |\theta|^2 \, dz\right]^{1/2}. \tag{37}$$

Hence, we obtain

$$\left[\int_0^1 |\theta|^2 \, dz\right]^{1/2} \geq \left[\int_0^1 |D\phi|^2 \, dz\right]^{1/2}. \tag{38}$$

By merging inequalities (36) and (38), we get

$$\int_0^1 |\theta|^2 \, dz \geq \int_0^1 \left(a^2 M_3 \, |\phi|^2 + |D\phi|^2\right) dz. \tag{39}$$

Since, $M_1 > 0$, $\epsilon > 0$ and $P_r > 0$ so from above inequality we deduce that

$$\epsilon M_1 P_r \left[\int_0^1 |\theta|^2 dz - \int_0^1 \left(a^2 M_3 \, |\phi|^2 + |D\phi|^2\right) dz\right] \geq 0. \tag{40}$$

Eq. (34) can be written as

$$\omega_i \left[\int_0^1 \left(|Dw|^2 + a^2|w|^2 + \epsilon P_r \, (1 + M_1) \, |\theta|^2 - \epsilon M_1 P_r \left(a^2 M_3 \, |\phi|^2 + |D\phi|^2\right)\right) dz\right] = 0. \tag{41}$$

Substituting inequality (40) into Eq. (41) confirms that the expression enclosed within the square brackets is strictly positive. This, in turn, leads to the conclusion that the imaginary part of the growth rate, ω_i, must vanish. The outcome affirms the validity of PES, indicating that the onset of convection is governed purely by a stationary (non-oscillatory) mode.

3 Mathematical Analysis

The initiation of convection is characterized by determining the critical value of the Rayleigh number, which marks the threshold at which the system departs from its stable equilibrium and enters a convective regime. According to the PES, this transition occur in a non-oscillatory manner, implying that the system evolves smoothly into a new steady state, wherein convection patterns become established.

Given that the instability arises in the form of steady convection, we consider the case where the growth rate $\omega = 0$. Substituting this condition into Eqs. (24), (26), and (27) simplifies the governing system to the following set of equations:

$$\left(\frac{\delta M_3 + 1}{k_0}\right) \left(D^2 - a^2\right) w = a\sqrt{R} \left(D\phi M_1 - (M_1 + 1) \, \theta\right), \tag{42}$$

$$\left(D^2 - a^2\right) \theta + P_r{}' M_2 \omega D\phi = (M_2 - 1) \sqrt{R} a w, \tag{43}$$

$$\left(D^2 - a^2 M_3\right) \phi - D\theta = 0, \tag{44}$$

We now proceed by applying the single-term Galerkin method, wherein only the leading term is retained in the series expansions for w, θ, and ϕ, following the approach outlined by Finlayson (2013).

Writing the variables w, θ, and ϕ appeared in Eqs. (42), (43) and (44) in terms of the following trial functions:

$$w = C_1 w_1, \quad \theta = C_2 \theta_1, \quad \text{and} \quad \phi = C_3 \phi_1. \tag{45}$$

Here, w_1, θ_1, and ϕ_1 represent appropriately chosen trial functions that satisfy the boundary conditions specified in Eqs. (28)–(31), and C_1, C_2, and C_3 are unknown constants to be determined.

Now, multiplying Eq. (42) by w_1, Eq. (43) by θ_1, and Eq. (44) by ϕ_1, respectively, and integrating the subsequent equations from $z = 0$ to $z = 1$, we get

$$\begin{aligned} C_1 \frac{(\delta M_3 + 1)}{k_0} \left(\int_0^1 w_1 \left(D^2 - a^2\right) w_1 dz\right) =& a\sqrt{R} M_1 C_3 \int_0^1 w_1 D\phi_1 dz \\ & - a\sqrt{R} C_2 \, (M_1 + 1) \int_0^1 w_1 \theta_1 dz, \end{aligned} \tag{46}$$

$$C_2 \int_0^1 \theta_1 \left(D^2 - a^2\right) \theta_1 dz = -\sqrt{R}aC_1 \int_0^1 w_1 \theta_1 dz, \tag{47}$$

$$C_3 \int_0^1 \phi_1 \left(D^2 - a^2\right) \phi_1 dz = C_2 \int_0^1 \phi_1 D\theta_1 dz. \tag{48}$$

After eliminating C_1, C_2, and C_3 from Eqs. (46) –(48), the expression for Rayleigh number is obtained as follows:

$$R = \frac{(\delta M_3 + 1)\, I_1 I_2 I_3}{a^2 k_0 I_4 \left[M_1 I_5 I_6 + (1 + M_1)\, I_1 I_4\right]}, \tag{49}$$

where

$$\begin{aligned}
I_1 &= \int_0^1 \left((D\phi_1)^2 + a^2 M_3 \phi_1^2\right) dz, \quad & I_2 &= \int_0^1 \left((D\theta_1)^2 + a^2 \theta_1^2\right) dz,\\
I_3 &= \int_0^1 \left((Dw_1)^2 + a^2 w_1^2\right) dz, & I_4 &= \int_0^1 w_1 \theta_1 dz,\\
I_5 &= \int_0^1 w_1 D\phi_1 dz, & I_6 &= \int_0^1 \phi_1 D\theta_1 dz.
\end{aligned}$$

The following algebraic polynomial trial functions are constructed to ensure compatibility with the boundary conditions defined in Eqs. (28)–(31):

$$w_1 = z^4 - (1 + h_1)\, z^3 + h_1 h_2 z^2 + h_1 (1 - h_2)\, z \tag{50}$$

$$\theta_1 = z^2 - z \tag{51}$$

$$\phi_1 = \frac{z^2}{2} - \frac{z^3}{3}. \tag{52}$$

where $h_1 = \frac{12+6K_0+2K_1+K_0K_1}{12+4(K_0+K_1)+K_0K_1}$ and $h_2 = \frac{K_0}{K_0+2}$.

By substituting the trial functions given in Eqs. (50)–(52) into the integrals I_1 through I_6, and evaluating each expression accordingly, the following results are obtained

$$\begin{aligned}
I_1 &= \frac{13M_3a^2 + 42}{1260}, \quad I_2 = \frac{a^2}{30} + \frac{1}{3},\\
I_3 &= \frac{h_1h_2}{5} - \frac{2h_1}{5} - \frac{13a^2h_1}{420} - h_1^2h_2 + \frac{a^2}{252} + \frac{4h_1^2}{5} + \frac{8a^2h_1^2}{105} + \frac{h_1^2h_2^2}{3} - \frac{a^2h_1^2h_2}{10}\\
&\quad + \frac{a^2h_1^2h_2^2}{30} + \frac{2a^2h_1h_2}{105} + \frac{3}{35},\\
I_4 &= \frac{h_1h_2}{30} - \frac{h_1}{20} + \frac{1}{105}, \quad I_5 = \frac{h_1}{20} - \frac{h_1h_2}{30} - \frac{1}{105}, \quad I_6 = \frac{1}{30}.
\end{aligned}$$

Substituting the evaluated values of the integrals I_1 through I_6 into Eq. (49) yields the following formulation for the Rayleigh number

$$R = \frac{(\delta M_3 + 1)\left(\frac{1}{3} + \frac{a^2}{30}\right)\left(A_1 + a^2A_2\right)\left(42 + 13a^2M_3\right)}{a^2k_0A_3\left[(1 + M_1)\, A_3\left(42 + 13a^2M_3\right) + 42M_1A_4\right]}, \tag{53}$$

where A_i's (i = 1 to 4) are given as

$$\begin{aligned}
A_1 &= \frac{3}{35} - \frac{2h_1}{5} + \frac{4h_1^2}{5} + \frac{h_1h_2}{5} + h_1^2h_2\left(\frac{h_2}{3} - 1\right),\\
A_2 &= \frac{1}{252} - \frac{13h_1}{420} + \frac{2h_1h_2}{105} + \frac{8h_1^2}{105} - \frac{h_1^2h_2}{10} + \frac{h_1^2h_2^2}{30},\\
A_3 &= \frac{1}{105} - \frac{h_1}{20} + \frac{h_1h_2}{30}, \quad A_4 = -\left(\frac{1}{105} - \frac{h_1}{20} + \frac{h_1h_2}{30}\right).
\end{aligned}$$

In the limit where M_1 assumes significantly large values, the influence of magnetic forces becomes dominant, effectively decoupling from the buoyancy-driven mechanism. Under such conditions, the corresponding magnetic Rayleigh number, defined as $N = RM_1$, is determined as follows:

$$N = \frac{(\delta M_3 + 1)\left(\frac{1}{3} + \frac{a^2}{30}\right)\left(A_1 + a^2 A_2\right)\left(42 + 13a^2 M_3\right)}{13 k_0 a^4 (A_3)^2 M_3}. \tag{54}$$

Eq. (54) is examined to determine the minimum value of the magnetic Rayleigh number N. This is achieved by locating the point at which N is stationary with respect to the wave number a, that is, by solving the condition $\frac{dN}{da} = 0$. The resulting equation is given below:

$$13A_3 M_3 a^6 - (130A_2 M_3 + 420A_3 + 42A_2)\, a^2 - 840A_2 = 0. \tag{55}$$

Solving Eq. (55) yields a positive root that corresponds to the critical wave number a_c, whose value depends on the parameters M_3, K_0, and K_1. It is important to highlight that obtaining a positive root of a from Eq. (55) is analytically challenging due to the complexity of the equation. Therefore, in this investigation, Eq. (55) has been addressed using a numerical approach implemented in MATLAB. The values of the critical wave number a_c are determined for selected parameter sets involving δ, M_3, k_0, K_0, and K_1. Once the critical wavenumber is computed, the corresponding magnetic Rayleigh numbers N_c are evaluated by substituting back into Eq. (55). These results are systematically presented in Tables 2 and 3. To ensure clarity and avoid redundancy, only representative results are displayed in the tables and figures, offering a concise yet comprehensive summary of the key findings.

3.1 Validation of the results

The chosen numerical method is validated by computing the wave number (a_c) and corresponding critical magnetic Rayleigh number (N_c) in the limiting case for particular values of M_3, k_0 and δ. The obtained values are then compared with the results reported by Prakash et al. (2018a) for ferrofluid layer saturating a densely packed porous medium. It is important to note that Prakash et al. (2018a) considered an idealized configuration with free-free boundary conditions and employed an analytical method by assuming sinusoidal trial functions to obtain an exact solution to the eigenvalue problem. Their approach is restricted to such ideal boundary scenarios and does not extend to more realistic boundaries. In contrast, the present study utilizes a single-term Galerkin method, which is a well-established and widely accepted technique for analyzing linear stability problems in hydrodynamic stability problems. Our formulation accommodates more generalized and physically realistic boundary conditions, such as permeable interfaces, for which the analytical method used by Prakash et al. (2018a) is not directly applicable. As a result, the Galerkin method yields approximate but highly reliable solutions.

Tab. 1: Comparative analysis of critical wave number (a_c) and critical magnetic Rayleigh number (N_c) in the present work and in Prakash's study for a ferrofluid layer for free-free bounding surfaces.

	$\delta = 0.03$, $k_0 = 0.0001$				$\delta = 0.07$, $k_0 = 0.0004$			
M_3	Present analysis		Prakash et al. (2018a)		Present analysis		Prakash et al. (2018a)	
	a_c	N_c	a_c	N_c	a_c	N_c	a_c	N_c
1	3.7941	5.3304 x 10^3	2	6.9525 x 10^3	3.7941	1.3844 x 10^3	2	1.8056 x 10^3
3	3.4286	4. 8945 x 10^3	1.4574	5.5495 x 10^3	3.4286	1.3583 x 10^3	1.4574	1.5401 x 10^3
5	3.3306	4.9859 x 10^3	1.3062	5.3995 x 10^3	3.3306	1.4633 x 10^3	1.3062	1.5846 x 10^3
7	3.2841	5.1625 x 10^3	1.2319	5.4602 x 10^3	3.2841	1.5893 x 10^3	1.2319	1.6809 x 10^3

The computed values of a_c and N_c in the present study show reasonably good agreement with those reported by Prakash et al. (2018a), despite minor deviations. These can be attributed to the methodological differences between the two approaches and the broader boundary conditions considered in the present analysis. Nevertheless, the close agreement in both trend and magnitude of the results confirms the accuracy and effectiveness for the current problem. Therefore, the comparison not only serves as a validation of the numerical approach but also highlights its suitability for handling more general physical configurations.

4 Numerical Approach

The present study employs the single-term Galerkin method (Finlayson (2013)) to solve the eigenvalue problem governing the onset of thermal instability in a ferrofluid layer saturated in a densely packed porous medium under the influence of magnetic field-dependent viscosity within permeable boundaries. This analytical technique is particularly well-suited for stability problems involving linear ordinary differential equations with boundary conditions, as it allows for a tractable yet accurate approximation of the solution through well-defined basis trail functions approach.

In applying this method, suitable trial functions are carefully selected to satisfy the corresponding boundary conditions for each perturbation quantities, including the velocity, temperature, and magnetic potential. These functions are substituted in the governing linearized, non-dimensional equations, which are then integrated across the domain of the system. This process results in an expression for the Rayleigh number in terms of the wave number and other physical parameters. The extremization of the resulting Rayleigh number expression with respect to the wave number yields a sixth-order algebraic equation, which is then numerically solved using MATLAB software. The positive real root of this equation gives the critical wave number a_c, which is then substituted back to compute the corresponding critical Rayleigh number. All numerical computations are carried out in MATLAB, which provides an efficient and reliable environment for symbolic manipulation, root-finding, and numerical plotting. MATLAB's symbolic toolbox is used to handle the algebraic manipulations involved in the Galerkin procedure, while its numerical solvers ensure precise computation of the eigenvalues. The graphical visualization of trends is also carried out in MATLAB. Tables summarizing the critical Rayleigh numbers and wave numbers for various parameter combinations are generated within the same framework to ensure consistency and clarity in the presentation of results.

5 Numerical Results and Discussion

The present work investigates the impact of magnetic-field-dependent (MFD) viscosity, boundary permeability, and magnetic parameters on the onset of thermal convection in a ferrofluid layer embedded in a porous medium. In this framework, the buoyancy-related magnetization parameter M_1 is taken to be significantly large, while M_2 is considered negligible, in accordance with the reasoning presented by Finlayson (1970). The parameter M_3, representing the nonlinearity in magnetization, is varied within the range of 1 to 15. Meanwhile, the viscosity contrast parameter δ is explored over the interval $0.01 \le \delta \le 0.09$, aligning with the parameter regimes employed in previous studies Prakash et al. (2018b); Sekar et al. (1993). For modeling the porous structure of the porous medium, the permeability values adopted are based on the data reported by Walker and Homsy (1977). The nature of the hydrodynamic boundary conditions is governed by the values of the parameters K_0 and K_1. Specifically, when both $K_0 \to 0$ and $K_1 \to 0$, the boundaries behave as dynamically free. In contrast, a configuration where $K_0 \to \infty$ (or $\ge 10^6$) and $K_1 \to 0$ corresponds to a free lower surface combined with a rigid upper surface. If both K_0 and K_1 approach infinity (or values exceeding 10^6), the boundaries are considered rigid. On the other hand, when K_0 and K_1 take finite values significantly less than 10^6, the system is characterized by semipermeable boundaries. To analyze the influence of these boundary conditions, critical parameters such as the magnetic Rayleigh number N_c and critical wavenumber a_c are evaluated numerically using MATLAB's symbolic computation capabilities. The accuracy of these results is ensured by benchmarking them against established findings in the literature. The impact of magnetization parameters, porous medium permeability, and MFD viscosity on N_c and a_c for each boundary configuration is elaborated in the subsequent discussion.

Case I: When $K_0 \to 0$, $K_1 \to 0$

When both boundaries are unrestricted or free, i.e., $K_0 \to 0$ and $K_1 \to 0$, we have $h_1 = 1$ and $h_2 = 0$. The expression for the magnetic Rayleigh number (N) in this case is given by

$$N = \frac{(1+\delta M_3)\left(\frac{1}{3}+\frac{a^2}{30}\right)\left(\frac{17}{35}+a^2\frac{31}{630}\right)(42+13a^2M_3)}{13k_0a^4\left(\frac{289}{176400}\right)M_3}.$$

Table 2 highlights the critical values of N_c and a_c for different boundary combinations associated with viscosity and magnetic parameters. In Fig. 2, the plot illustrates the connection between viscosity parameter (δ) and critical magnetic Rayleigh number (N_c) for $M_3 = 1, 10$. The findings demonstrate that an increase in δ leads to a continuous rise in N_c, implying that viscosity delays the onset of convection for free-free boundary combinations.This is because higher viscosity increases the internal resistance to fluid motion, thereby suppressing convective disturbances and requiring a higher thermal gradient (i.e., a higher N_c) to initiate instability. From Figures 3(a) and 3(b), it is observed that the parameter M_3 exhibits a dual effect on the system. For each curve corresponding to a fixed δ, the critical magnetic Rayleigh number N_c initially decreases with increasing M_3, reaches a minimum, and then increases steadily. As the magnetic field strengthens, it enhances both magnetization and viscosity. While magnetization promotes instability, the increased viscosity suppresses it. This shift leads to a stabilizing influence, resulting in a higher critical magnetic Rayleigh number. Hence, the net effect of M_3 varies depending on the dominance of either mechanism, reflecting its dual nature. The effect is more prominent for larger values of δ, as MFD further enhances the internal resistance to motion, thereby delaying the onset of convection. Also, the effect of M_1 is discussed in Fig. 4. The results clearly indicate that the Rayleigh number falls as M_1 values increase, thus establishing that M_1 creates instability within the system.

Case II: When $K_0 \to \infty$, $K_1 \to \infty$

In the case where both bounding surfaces are considered perfectly rigid, that is, $K_0 \to \infty$ and $K_1 \to \infty$, the parameters take the values $h_1 = 1$ and $h_2 = 1$. Under these conditions, the corresponding expression for N is obtained as:

$$N = \frac{19600(1+\delta M_3)\left(\frac{1}{3}+\frac{a^2}{30}\right)\left(\frac{24}{35}-\frac{133a^2}{1260}\right)(42+13a^2M_3)}{13k_0a^4M_3}.$$

In Table 2, the values of N_c and a_c are listed for various combinations of δ and M_3 for rigid–rigid boundary conditions. Figure 2 shows that increasing δ leads to a monotonic rise in N_c, indicating a stabilizing effect due to enhanced viscous resistance. Furthermore, Figures 3(a) and 3(b) reveal that M_3 exhibits a dual influence: for each fixed δ, N_c first decreases and then increases with increasing M_3. This behavior is similar to that observed for free–free boundaries; however, the values of N_c are comparatively

Tab. 2: Variation of critical magnetic Rayleigh number (N_c) with critical wave number (a_c) for distinct values of δ, and M_3 for different boundary combinations.

δ	M_3	Free-Free ($K_0 = K_1 = 0$)		Rigid-Free ($K_0 = 10^6, K_1 = 0$)		Rigid-Rigid ($K_0 = K_1 = 10^6$)	
		a_c	$(N_{ff})_c$	a_c	$(N_{rf})_c$	a_c	$(N_{rr})_c$
0.01	1	3.7941	50914.9335	3.8987	56603.9770	3.9402	57263.6907
	5	3.3306	44344.5784	3.4392	49741.1290	3.4820	50489.3356
	10	3.2472	45147.0070	3.3577	50729.4455	3.4011	51525.5945
	15	3.2170	46727.1646	3.3283	52538.6217	3.3720	53375.7127
0.03	1	3.7941	51923.1500	3.8987	57724.8479	3.9402	58397.6252
	5	3.3306	48567.8716	3.4392	54478.3794	3.4820	55297.8438
	10	3.2472	53355.5537	3.3577	59952.9810	3.4011	60893.8844
	15	3.2170	58916.8597	3.3283	66244.3491	3.3720	67299.8117
0.05	1	3.7941	52931.3665	3.8987	58845.7187	3.9402	59531.5597
	5	3.3306	52791.1648	3.4392	59215.6297	3.4820	60106.3519
	10	3.2472	61564.1004	3.3577	69176.5166	3.4011	70262.1743
	15	3.2170	71106.5548	3.3283	79950.0765	3.3720	81223.9107
0.07	1	3.7941	53939.5831	3.8987	59966.5895	3.9402	60665.4941
	5	3.3306	57014.4580	3.4392	63952.8801	3.4820	64914.8601
	10	3.2472	69772.6471	3.3577	78400.0521	3.4011	79630.4642
	15	3.2170	83296.2499	3.3283	93655.8039	3.3720	95148.0097
0.09	1	3.7941	54947.7996	3.8987	61087.4603	3.9402	61799.4286
	5	3.3306	61237.7511	3.4392	68690.1305	3.4820	69723.3682
	10	3.2472	77981.1939	3.3577	87623.5877	3.4011	88998.7541
	15	3.2170	95485.9450	3.3283	107361.5313	3.3720	109072.1086

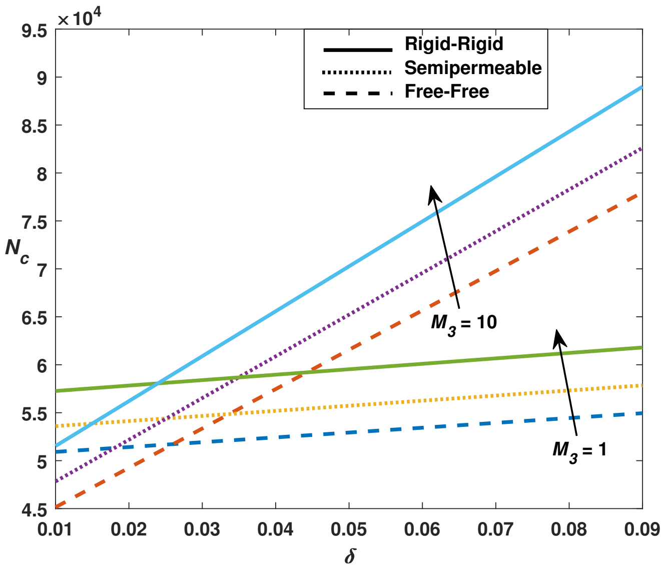

Fig. 2: Variation of N_c with δ for different M_3, and $k_0 = 0.001$.

higher in the rigid–rigid case due to stronger mechanical constraints at the boundaries, which resist fluid motion more effectively and delay the onset of convection.

Case III: When $K_0 \neq 0$ (finite) and $K_1 \neq 0$ (finite)

When both boundary surfaces are semipermeable with finite values of the parameters K_0 and K_1 greater than zero—the mathematical form of N remains unchanged and is still represented by Eq. (54).

Table 3 presents computed values of the critical magnetic Rayleigh number N_c and the corresponding critical wavenumber a_c for various combinations of the viscosity-related parameter δ and the magnetization parameter M_3. As shown in Figures 2, 3(a), and 3(b), the trends observed for δ and M_3 align with those discussed earlier in Cases I and II. A comparative analysis of Tables 2 and 3, along with these figures, reveals that the critical values N_c and a_c under semipermeable boundary conditions fall between the values obtained for the limiting cases of free-free and rigid-rigid boundaries. This observation suggests that the

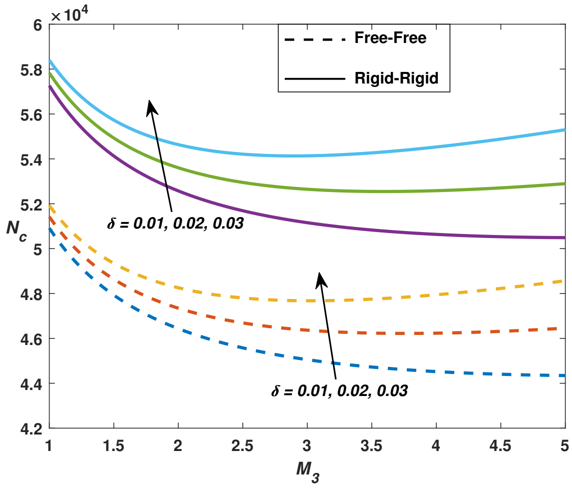

(a)

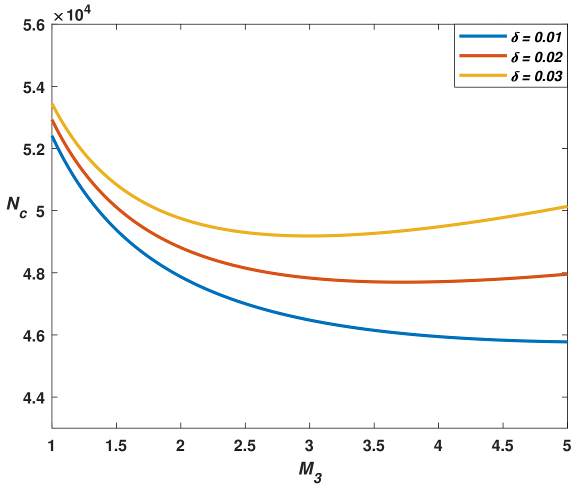

(b)

Fig. 3: Variation of N_c with M_3 for distinct δ values for (a) free-free and rigid-rigid boundaries (b) semipermeable boundaries.

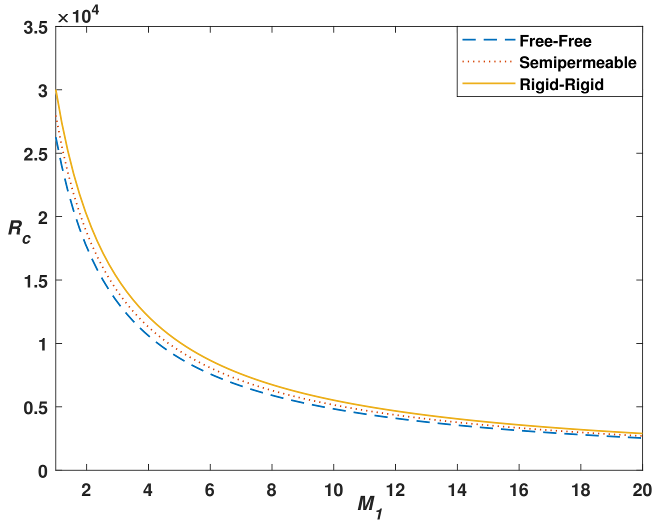

Fig. 4: Variation of R_c versus M_1 for free-free, semipermeable and rigid-rigid boundaries.

onset of thermal convection is delayed in rigid boundary settings compared to free boundaries, with semipermeable boundaries yielding intermediate behavior. Moreover, Figure 4 confirms that the magnetization parameter M_1 continues to have a destabilizing influence on the system even in this configuration.

Case IV: When $K_0 \to \infty$, $K_1 \to 0$

For the scenario involving a rigid lower surface and a free upper surface—mathematically represented by $K_0 \to \infty$ and $K_1 \to 0$—the corresponding parameter values are $h_1 = \frac{3}{2}$ and $h_2 = 1$. Under this boundary configuration, the magnetic Rayleigh number N is obtained using the following expression:

$$N = \frac{705600(1+\delta M_3)\left(\frac{1}{3}+\frac{a^2}{30}\right)\left(-\frac{31}{14}-\frac{97a^2}{1260}\right)(42+13a^2M_3)}{13k_0a^4M_3}.$$

The numerical results for N_c and a_c for this case are presented in Table 2. The trends in the critical magnetic Rayleigh numbers are consistent with those observed in the previously discussed Cases I, II, and III. Trends for the viscosity parameter (δ) as well as the magnetic parameters M_1 and M_3, similarly suggest that the system behaves uniformly under different boundary conditions (corresponding graphs are excluded for brevity of the manuscript).
Table 2 contains the computed values of N_c and a_c for this particular configuration. The observed variations in N_c align well with the patterns established in Cases I, II, and III discussed earlier. The influence of the viscosity parameter δ and the magnetic parameters M_1 and M_3 also display consistent behavior across the various boundary scenarios considered. To maintain clarity, corresponding graphical illustrations have been omitted from the manuscript.

From all the cases discussed above, it can be concluded that a transition in the permeable boundaries from free to rigid

Tab. 3: Variation of critical magnetic Rayleigh numbers (N_c) with critical wave number (a_c) for different values of δ and M_3 for partially permeable boundaries.

K_0	K_1	M_3	$\delta = 0.01$		$\delta = 0.03$		$\delta = 0.05$		$\delta = 0.07$	
			a_c	N_c	a_c	N_c	a_c	N_c	a_c	N_c
		1	3.7940	50918.2428	3.7940	51926.5249	3.7940	52934.8069	3.7940	53943.0889
		5	3.3305	44347.2443	3.3305	48570.7914	3.3305	52794.3385	3.3305	57017.8855
0.1	0.1	10	3.2471	45149.6776	3.2471	53358.7099	3.2471	61567.7422	3.2471	69776.7745
		15	3.2169	46729.9121	3.2169	58920.3239	3.2169	71110.7357	3.2169	83301.1476
		1	3.7942	50938.0093	3.7942	51946.6827	3.7942	52955.3562	3.7942	53964.0296
		5	3.3307	44365.1861	3.3307	48590.4419	3.3307	52815.6978	3.3307	57040.9536
0.1	0.5	10	3.2473	45168.0901	3.2473	53380.4701	3.2473	61592.8501	3.2473	69805.2301
		15	3.2171	46749.0247	3.2171	58944.4225	3.2171	71139.8202	3.2171	83335.2180
		1	3.7946	50981.5476	3.7946	51991.0832	3.7946	53000.6188	3.7946	54010.1543
		5	3.3311	44404.4930	3.3311	48633.4924	3.3311	52862.4917	3.3311	57091.4910
1	1	10	3.2477	45208.3871	3.2477	53428.0938	3.2477	61647.8006	3.2477	69867.5073
		15	3.2175	46790.8387	3.2175	58997.1444	3.2175	71203.4501	3.2175	83409.7559
		1	3.8216	52360.4750	3.8216	53397.3161	3.8216	54434.1572	3.8216	55470.9983
		5	3.3592	45713.7588	3.3592	50067.4501	3.3592	54421.1415	3.3592	58774.8328
1	10	10	3.2763	46563.0764	3.2763	55029.0903	3.2763	63495.1042	3.2763	71961.1181
		15	3.2463	48201.2386	3.2463	60775.4748	3.2463	73349.7109	3.2463	85923.9471
		1	3.8268	52408.6258	3.8268	53446.4204	3.8268	54484.2150	3.8268	55522.0096
		5	3.3646	45776.4446	3.3646	50136.1060	3.3646	54495.7674	3.3646	58855.4288
10	10	10	3.2818	46631.0524	3.2818	55109.4256	3.2818	63587.7987	3.2818	72066.1719
		15	3.2519	48273.1792	3.2519	60866.1824	3.2519	73459.1857	3.2519	86052.1890
		1	3.9252	56606.3331	3.9252	57727.2505	3.9252	58848.1680	3.9252	59969.0855
		5	3.4666	49850.0629	3.4666	54597.6880	3.4666	59345.3130	3.4666	64092.9381
10^2	10^3	10	3.3854	50861.5408	3.3854	60109.0937	3.3854	69356.6465	3.3854	78604.1994
		15	3.3562	52683.3962	3.3562	66426.8908	3.3562	80170.3855	3.3562	93913.8802
		1	3.9385	57189.0424	3.9385	58321.4987	3.9385	59453.9550	3.9385	60586.4113
		5	3.4803	50416.8002	3.4803	55218.4002	3.4803	60020.0002	3.4803	64821.6003
10^3	10^4	10	3.3994	51450.2587	3.3994	60804.8512	3.3994	70159.4437	3.3994	79514.0362
		15	3.3702	53297.1750	3.3702	67200.7858	3.3702	81104.3967	3.3702	95008.0076

results in an increase in the critical magnetic Rayleigh number, which signifies greater stability in the system. Also, M_1 induces a destabilizing influence within the system. This behavior may result from the stronger destabilizing magnetic force, as ferrofluids exhibit better heat transport than standard fluids. For lower M_3 values, M_3 also has a destabilizing effect on the onset of stationary convection for all cases of boundary conditions. This may be due to the large pyromagnetic coefficient or large temperature gradient. Similar behavior of M_1 and M_3 have been observed and documented by numerous researchers in the study of convective instability in ferrofluids (Dhiman and Sharma (2021); Finlayson (1970); Prakash et al. (2018b)).

Also, Figures 5(a) and 5(b) illustrate the variation of a_c versus M_1 and a_c versus M_3 respectively for different boundary combinations, with fixed values of $\delta = 0.03$ for $k_0 = 0.001$. As shown in Fig. 5(a), the critical wave number (a_c) rises with increasing magnetic number (M_1), resulting a contraction in the dimensions of convection cells. This suggests that enhanced strength of the magnetic field intensity results in tighter and more organized convection cells, fostering a more stable and organized flow in the fluid layer. On the other hand, from Fig. 5(b) it is apparent that as M_3 increases, the critical wave number (a_c) decreases for each case of boundary combinations. This decline in wave number signifies a concurrent increase in the size of convection cells. Fig. 6 describes the relationship between porous medium permeability k_0 and critical magnetic Rayleigh number (N_c) for $\delta = 0.03$ and $M_3 = 5$. The data show that (k_0) has an inverse relation with the magnetic Rayleigh number, suggesting that higher medium permeability destabilizes the system. This occurs because higher medium permeability enhances the void fraction, thereby facilitating greater fluid motion in the direction normal to the boundary planes. Consequently, the enhanced heat transport leads to the earlier onset of convection.

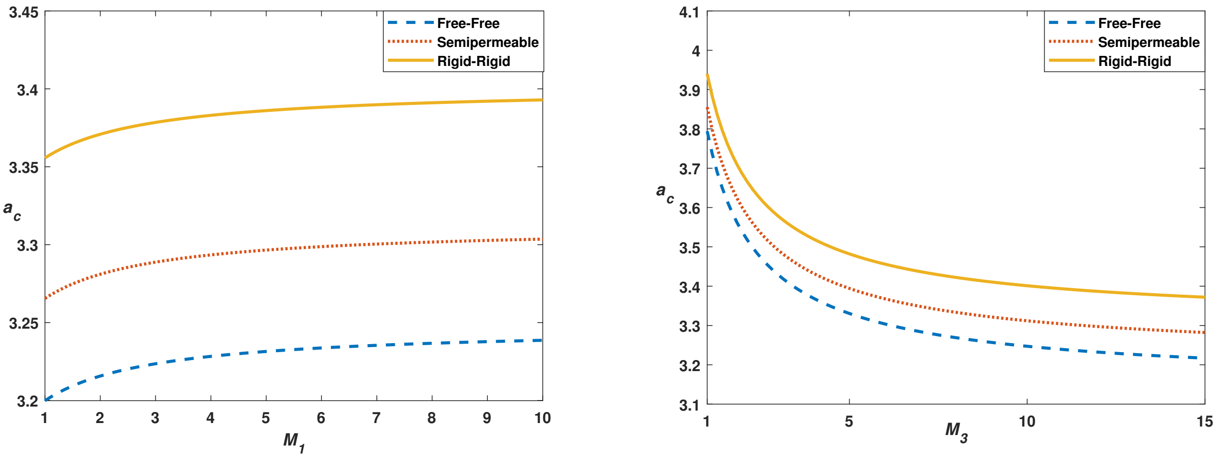

(a) Variation of a_c versus M_1.

(b) Variation of a_c versus M_3.

Fig. 5: Variation of a_c with M_1 and M_3 for fixed values of $\delta = 0.03$ and $k_0 = 0.001$.

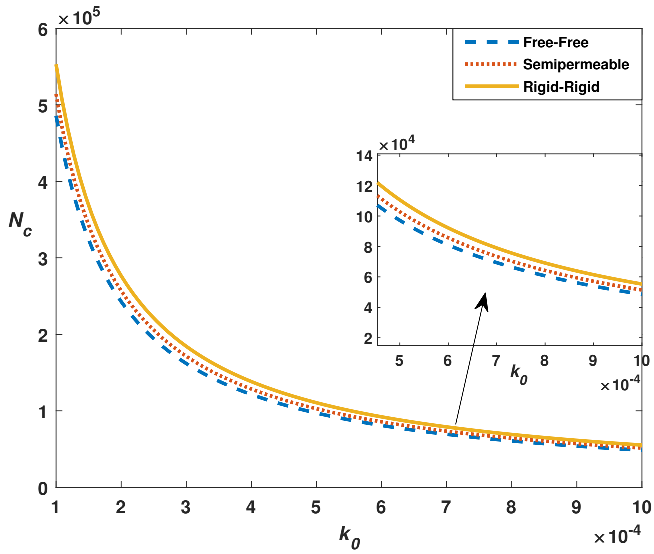

Fig. 6: Plot of N_c against k_0 with $\delta = 0.03$ and $M_3 = 5$.

Figures 7(a) and 7(b) provide significant insights into the neutral stability region. The graph illustrates the relationship between the wave number (a), permeability parameter K of the bounding surfaces, and the magnetic Rayleigh number (N). Fig. 7(a) shows an equal variation in permeability for both bounding surfaces i.e. $K_0 = K_1$. The area below this region signifies a stable state.

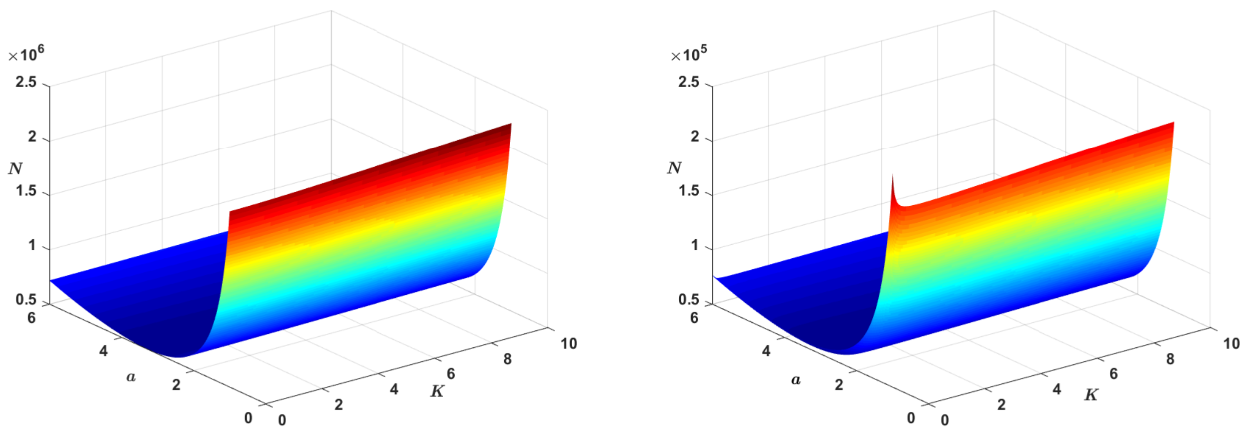

(a) Assuming equal boundary permeabilities $K_0 = K_1$.

(b) Assuming boundary permeabilities $K_0 = \frac{1}{K_1}$.

Fig. 7: Dependence of N on a for selected K values at constant $M_3 = 7$, $k_0 = 0.001$.

It is evident from Fig. 7(a) that the curvature consistently rises with an increase in K, indicating that the system becomes more stable as rigidity approaches. However, when permeability of the upper boundary is inversely proportional to the permeability of the lower boundary i.e. $K_1 \propto \frac{1}{K_0}$ (see Fig. 7(b)), then it is observed that the permeability of the boundaries has a destabilizing influence on the system within the range from 0 to 1, with the highest level of instability occurring when K is approximately one. This observation closely aligns with the findings reported by Gupta et al. (2013) on classical Rayleigh-Bénard convection with permeable boundaries.

6 Conclusive Remarks

This research fundamentally explores the influence of several key factors on the onset of convection in a ferrofluid layer that is dispersed throughout a densely packed porous medium under an external uniform magnetic field. The fluid layer is embedded between two horizontal permeable boundaries, and the Galerkin method is adopted to numerically address the eigenvalue problem. The results obtained through this numerical analysis demonstrate excellent agreement with previously published works on this topic. The conclusive remarks of this study are as follows:

1. The MFD viscosity parameter (δ) postpones the initiation of ferromagnetic convection in ferrofluid layer. Therefore, as δ increases, it slowdowns the convection, enhancing the system's stability and necessitating higher values of R_c for convection to arise. In the presence of the magnetic field, this resistance to flow causes convection to develop more slowly compared to the absence of a magnetic field.
2. The Rayleigh number (R) and the magnetic number M_1 exhibit an inverse proportionality. This inverse relationship enhances the fluid's ability to respond to magnetic fields, leading to enhanced heat transfer and fluid flow. This leads to convection being initiated at weaker thermal driving forces. Recognizing this correlation can be beneficial in the design and optimization of magnetic fluid-based systems, where the accurate control of heat transfer and fluid motion is a crucial factor.
3. Smaller values of M_3 exhibit a destabilizing effect on the system, whereas higher values tend to stabilize the flow, highlighting its contrasting behavior. This dual role becomes increasingly evident as the system approaches rigidity. Furthermore, M_3 is found to widen the convection cells.
4. Under identical physical conditions, the critical magnetic Rayleigh number is found to be the lowest for free-free boundary configurations, while it attains the highest value when both boundaries are rigid. In the case of semi-permeable boundaries, the critical value lies between those of the free-free and rigid-rigid cases. This leads to the ordering: $(N_{ff})_c < (N_{sp})_c < (N_{rr})_c$, where $(N_{sp})_c$ represents the critical magnetic Rayleigh number corresponding to semi-permeable boundaries.
5. The boundaries permeability significantly affects the stability of the system i.e., the system exhibits stronger stabilization for rigid boundaries ($K_0 = K_1 \to \infty$), while weak stabilization is noted for free boundaries ($K_0 = K_1 = 0$).

This study provides significant insight into the role of MFD viscosity, porous media permeability, and variations in permeable boundaries in affecting the system.The core contribution lies in demonstrating how these coupled physical factors influence the onset of thermal convection and system stability in a porous medium. The analysis delivers reliable predictions while offering deeper physical insight into the role of boundary behavior and magnetic control. The results have direct implications for optimizing ferrofluid-based applications where precise thermal regulation and fluids movement control are essential. However, additional research is needed to broaden the analysis. Future work could delve into non-linear stability and transient convection to gain a more comprehensive understanding of the system's behavior beyond its initial instability. Furthermore, examining non-isothermal conditions and the effects of different magnetic field orientations, such as angled or time-varying fields, would make the findings more relevant for practical applications. Studying other ferrofluid characteristics, like non-Newtonian properties and temperature-sensitive viscosity, could also bring new stability features to light.

References

Gordon S Beavers and Daniel D Joseph. Boundary conditions at a naturally permeable wall. *Journal of fluid mechanics*, 30(1): 197–207, 1967.

Subrahmanyan Chandrasekhar. *Hydrodynamic and hydromagnetic stability*. Courier Corporation, 2013.

JOGINDER SINGH Dhiman and NIVEDITA Sharma. Effect of temperature dependent viscosity on thermal convection in ferrofluid layer. *Journal of Theoretical and Applied Mechanics*, 51(1):3–21, 2021.

R Ellahi. The effects of mhd and temperature dependent viscosity on the flow of non-newtonian nanofluid in a pipe: analytical solutions. *Applied Mathematical Modelling*, 37(3):1451–1467, 2013.

BA0191 Finlayson. Convective instability of ferromagnetic fluids. *Journal of Fluid Mechanics*, 40(4):753–767, 1970.

Bruce A Finlayson. *The method of weighted residuals and variational principles*. SIAM, 2013.

AK Gupta and RG Shandil. On the existence of hydrodynamic instability in single diffusive bottom heavy systems with permeable boundaries. *Proceedings-Mathematical Sciences*, 121:495–501, 2011.

AK Gupta, RG Shandil, and Sohan Kumar. On Rayleigh Bénard convection with porous boundaries. *Proceedings of the National Academy of Sciences, India Section A: Physical Sciences*, 83:365–369, 2013.

Mohsen Izadi, Masoud Javanahram, Seyed Mohsen Hashem Zadeh, and Dengwei Jing. Hydrodynamic and heat transfer properties of magnetic fluid in porous medium considering nanoparticle shapes and magnetic field-dependent viscosity. *Chinese Journal of Chemical Engineering*, 28(2):329–339, 2020.

Daniel J Keene and RJ Goldstein. Thermal convection in porous media at high Rayleigh numbers. *Journal of Heat Transfer*, 137 (3):034503, 2015.

M Kpossa and AV Monwanou. Combined effects of helical force and rotation on stationary convection of a binary ferrofluid in a porous medium. *International Journal of Applied Mechanics and Engineering*, 27(2):158–176, 2022.

Pankaj Kumar, Mandeep Kaur, Abhishek Thakur, and Renu Bala. On estimating the growth rate of perturbations in rivlin-ericksen ferromagnetic convection with magnetic field dependent viscosity. *Technische Mechanik-European Journal of Engineering Mechanics*, 44(1):1–13, 2024a.

Pankaj Kumar, Awneesh Kumar, and Abhishek Thakur. Effect of viscosity variation with temperature on convective instability in a hot dusty ferrofluid layer with permeable boundaries. *Numerical Heat Transfer, Part B: Fundamentals*, pages 1–18, 2024b.

Pankaj Kumar, Abhishek Thakur, Mandeep Kaur, and Awneesh Kumar. Numerical investigation of the impact of magnetic field dependent viscosity on darcy–brinkman ferromagnetic convection with permeable boundaries. *Special Topics & Reviews in Porous Media: An International Journal*, 16(4), 2025.

Chitresh Kumari, Jitender Kumar, and Jyoti Prakash. The onset of electrothermoconvection in a viscoelastic dielectric fluid layer with internal heat source: Navier-stokes-voigt model. *Technische Mechanik-European Journal of Engineering Mechanics*, 44(4), 2024.

DP Lalas and S Carmi. Thermoconvective stability of ferrofluids. *The Physics of Fluids*, 14(2):436–438, 1971.

US Mahabaleshwar, KN Sneha, A Chan, and Dia Zeidan. An effect of mhd fluid flow heat transfer using cnts with thermal radiation and heat source/sink across a stretching/shrinking sheet. *International Communications in Heat and Mass Transfer*, 135:106080, 2022.

US Mahabaleshwar, T Anusha, SM Sachhin, Dia Zeidan, and Sang Woo Joo. An impact of richardson number on the inclined mhd mixed convective flow with heat and mass transfer. *Heat Transfer*, 53(6):3104–3124, 2024.

Amit Mahajan and Monika Arora. Convection in rotating magnetic nanofluids. *Applied Mathematics and Computation*, 219(11): 6284–6296, 2013.

Amit Mahajan and Mahesh Kumar Sharma. Convection in magnetic nanofluids in porous media. *Journal of Porous Media*, 17(5): 439–455, 2014.

M Molana, AS Dogonchi, T Armaghani, Ali J Chamkha, DD Ganji, and Iskander Tlili. Investigation of hydrothermal behavior of Fe_3O_4-H_2O nanofluid natural convection in a novel shape of porous cavity subjected to magnetic field dependent (MFD) viscosity. *Journal of Energy Storage*, 30:101395, 2020.

CE Nanjundappa, IS Shivakumara, and HN Prakash. Effect of coriolis force on thermomagnetic convection in a ferrofluid saturating porous medium: A weakly nonlinear stability analysis. *Journal of magnetism and magnetic materials*, 370:140–149, 2014.

Donald A Nield and Adrian Bejan. *Convection in porous media*, volume 3. Springer, 2006.

Kandavkovi Mallikarjuna Nihaal, Ulavathi Shettar Mahabaleshwar, Dia Zeidan, and Sang Woo Joo. Impact of quadratic thermal radiation on mhd nanofluid flow across a stretching sheet with variable thickness: Xue and yamado-ota thermophysical model. *Acta Mechanica Sinica*, 41(6):724405, 2025.

Stefan Odenbach and Steffen Thurm. Magnetoviscous effects in ferrofluids. In *Ferrofluids: magnetically controllable fluids and their applications*, pages 185–201. Springer, 2002.

Anne Pellew and Richard Vynne Southwell. On maintained convective motion in a fluid heated from below. *Proceedings of the Royal Society of London. Series A. Mathematical and Physical Sciences*, 176(966):312–343, 1940.

Jyoti Prakash, Pankaj Kumar, Kultaran Kumari, and Shweta Manan. Ferromagnetic convection in a densely packed porous medium with magnetic-field-dependent viscosity–revisited. *Zeitschrift für Naturforschung A*, 73(3):181–189, 2018a.

Jyoti Prakash, Shweta Manan, and Pankaj Kumar. Ferromagnetic convection in a sparsely distributed porous medium with magnetic field dependent viscosity revisited. *Journal of Porous Media*, 21(8):749–762, 2018b.

Kaka Ram, Jitender Thakur, Pankaj Kumar, and Jyoti Prakash. On the complex growth rate of a perturbation in ferrothermohaline convection with magnetic-field-dependent viscosity in a densely packed porous medium. *Special Topics & Reviews in Porous Media: An International Journal*, 12(3):89–104, 2021.

Kaka Ram, Jyoti Prakash, Kultaran Kumari, and Pankaj Kumar. Upper bounds for the complex growth rate of a disturbance in ferrothermohaline convection. *Studia Geotechnica et Mechanica*, 44(2):114–122, 2022.

Paras Ram, Anupam Bhandari, and Kushal Sharma. Effect of magnetic field-dependent viscosity on revolving ferrofluid. *Journal of Magnetism and Magnetic materials*, 322(21):3476–3480, 2010.

Ronald E Rosensweig. *Ferrohydrodynamics*. Courier Corporation, 1997.

SM Sachhin, US Mahabaleshwar, HN Huang, B Sunden, and Dia Zeidan. An influence of temperature jump and navier's slip-on hybrid nano fluid flow over a permeable stretching/shrinking sheet with heat transfer and inclined mhd. *Nanotechnology*, 35(11): 115401, 2023.

L Schwab, U Hildebrandt, and K Stierstadt. Magnetic Bénard convection. *Journal of Magnetism and Magnetic Materials*, 39(1-2): 113–114, 1983.

R Sekar, G Vaidyanathan, and A Ramanathan. The ferroconvection in fluids saturating a rotating densely packed porous medium. *International journal of engineering science*, 31(2):241–250, 1993.

Fatih Selimefendigil and Hakan F Öztop. Numerical study and pod-based prediction of natural convection in a ferrofluids–filled triangular cavity with generalized neural networks. *Numerical Heat Transfer, Part A: Applications*, 67(10):1136–1161, 2015.

Poonam Sharma, Amit Mahajan, et al. A nonlinear stability analysis for thermoconvective magnetized ferrofluid with magnetic-field-dependent viscosity saturating a porous medium. *Journal of Porous Media*, 12(7):667–682, 2009.

M Sheikholeslami, MM Rashidi, T Hayat, and DD Ganji. Free convection of magnetic nanofluid considering MFD viscosity effect. *Journal of Molecular Liquids*, 218:393–399, 2016.

Mark Isaakovich Shliomis. Magnetic fluids. *Soviet Physics Uspekhi*, 17(2):153, 1974.

Venkatesh Vidya Shree, Chandrappa Rudresha, Chandrashekar Balaji, and Sokalingam Maruthamanikandan. Effect of magnetic field dependent viscosity on darcy-brinkman ferroconvection with second sound. *East European Journal of Physics*, (4): 112–117, 2022.

Pradeep G Siddheshwar. Convective instability of ferromagnetic fluids bounded by fluid-permeable, magnetic boundaries. *Journal of magnetism and magnetic materials*, 149(1-2):148–150, 1995.

Peter J Stiles and Michael Kagan. Thermoconvective instability of a horizontal layer of ferrofluid in a strong vertical magnetic field. *Journal of Magnetism and Magnetic Materials*, 85(1-3):196–198, 1990.

D Surya and AK Gupta. Thermal instability in a liquid layer with permeable boundaries under the influence of variable gravity. *European Journal of Mechanics-B/Fluids*, 91:219–225, 2022.

Kambiz Vafai. Convective flow and heat transfer in variable-porosity media. *Journal of fluid mechanics*, 147:233–259, 1984.

Kambiz Vafai. *Handbook of porous media*. Crc Press, 2015.

S Venkatasubramanian and PN Kaloni. Effects of rotation on the thermoconvective instability of a horizontal layer of ferrofluids. *International journal of engineering science*, 32(2):237–256, 1994.

AB Vishalakshi, Ulavathi Shettar Mahabaleshwar, V Anitha, and Dia Zeidan. A nanofluid couple stress flow due to porous stretching and shrinking sheet with heat transfer. *Journal of Porous Media*, 27(8), 2024.

Angadi Basettappa Vishalakshi, Ulavathi Shettar Mahabaleshwar, David Laroze, and Dia Zeidan. A study of mixed convective ternary hybrid nanofluid flow over a stretching sheet with radiation and transpiration. *Special Topics & Reviews in Porous Media: An International Journal*, 14(2), 2023.

K Walker and GM Homsy. A note on convective instabilities in Boussinesq fluids and porous media. *Journal of Heat and Mass Transfer*, 99(2):338–339, 1977.

Ahmad Zeeshan, Nouman Khalid, Rahmat Ellahi, MI Khan, and Sultan Z Alamri. Analysis of nonlinear complex heat transfer mhd flow of jeffrey nanofluid over an exponentially stretching sheet via three phase artificial intelligence and machine learning techniques. *Chaos, Solitons & Fractals*, 189:115600, 2024.

Dia Zeidan, R Touma, and A Slaouti. Implementation of velocity and pressure non-equilibrium in gas-liquid two-phase flow computations. *International Journal of Fluid Mechanics Research*, 41(6), 2014.